


















Continuous-wave two-photon terahertz quantum cascade laser

R. A. Khabibullin ; D. V. Ushakov ; A. A. Afonenko ; A. Yu. Pavlov ; R. R. Galiev ;
D. S. Ponomarev ; A. P. Vasilyev; A. G. Kuzmenkov ; N. A. Maleev ; F. I. Zubov ; M. V. Maksimov ;
D. A. Belov ; A. V. Ikonnikov ; D. I. Kuritsyn; R. Kh. Zhukavin ; K. A. Kovalevsky; V. A. Anferte; V. L. Vaks; A. V. Antonov; A. A. Dubinov ; S. V. Morozov ; V. I. Gavrilenko  



J. Appl. Phys. 136, 194504 (2024)

<https://doi.org/10.1063/5.0230491>



Articles You May Be Interested In

Limiting factors to the performance and operation frequency range of THz quantum cascade laser based on GaAs/AlGaAs heterostructures

AIP Conference Proceedings (June 2021)

Feasibility of GaAs/AlGaAs quantum cascade laser operating above 6 THz

J. Appl. Phys. (April 2024)

Subterahertz difference-frequency generation in terahertz quantum cascade lasers

Appl. Phys. Lett. (December 2022)

Continuous-wave two-photon terahertz quantum cascade laser

Cite as: J. Appl. Phys. **136**, 194504 (2024); doi: [10.1063/5.0230491](https://doi.org/10.1063/5.0230491)

Submitted: 24 July 2024 · Accepted: 5 November 2024 ·

Published Online: 20 November 2024



R. A. Khabibullin,^{1,2} D. V. Ushakov,³ A. A. Afonenko,³ A. Yu. Pavlov,¹ R. R. Galiev,^{1,4} D. S. Ponomarev,¹ A. P. Vasilyev,⁵ A. G. Kuzmenkov,⁴ N. A. Maleev,⁴ F. I. Zubov,⁶ M. V. Maksimov,⁶ D. A. Belov,⁷ A. V. Ikonnikov,⁷ D. I. Kuritsyn,⁸ R. Kh. Zhukavin,⁸ K. A. Kovalevsky,⁸ V. A. Anfertev,⁸ V. L. Vaks,^{8,9} A. V. Antonov,⁸ A. A. Dubinov,^{8,9} S. V. Morozov,^{8,9} and V. I. Gavrilenko^{8,10,a)}

AFFILIATIONS

¹Mokerov Institute of Ultrahigh Frequency Semiconductor Electronics, Moscow 117105, Russia

²Moscow Institute of Physics and Technology, Moscow 117303, Russia

³Department of Radiophysics and Computer Technologies, Belarusian State University, Minsk 220030, Belarus

⁴Ioffe Institute, Saint Petersburg 194021, Russia

⁵Research & Engineering Center, RAS, Submicron Heterostructures for Microelectronics, Saint Petersburg 194021, Russia

⁶Laboratory of Nanophotonics, Alferov University, Saint Petersburg 194021, Russia

⁷Physics Department, M.V. Lomonosov Moscow State University, Moscow 119991, Russia

⁸Institute for Physics of Microstructures, Russian Academy of Sciences, Nizhny Novgorod 603950, Russia

⁹Department of Radiophysics, Lobachevsky State University, Nizhny Novgorod 603022, Russia

¹⁰Advanced School of General and Applied Physics, Lobachevsky State University, Nizhny Novgorod 603022, Russia

^{a)}Author to whom correspondence should be addressed: gavr@ipmras.ru

ABSTRACT

We report on the implementation of a terahertz two-photon quantum cascade laser operating in a continuous wave mode. Lasers that can emit two photons as a result of the relaxation of a single electron between two states of the same parity have been discussed since the early days of the laser era, but implementation has been hampered by the lack of a suitable gain medium. The semiconductor structure of a quantum cascade laser seems to be an ideal medium for realizing such two-photon emission. Our work demonstrates dual-band laser radiation in the range of 3.1–3.9 THz (104–130 cm^{−1}) at temperatures up to 90 K.

© 2024 Author(s). All article content, except where otherwise noted, is licensed under a Creative Commons Attribution-NonCommercial-NoDerivs 4.0 International (CC BY-NC-ND) license (<https://creativecommons.org/licenses/by-nc-nd/4.0/>). <https://doi.org/10.1063/5.0230491>

I. INTRODUCTION

Quantum cascade lasers (QCLs), operating on electron transitions between the states arising from size quantization in GaAs/AlGaAs quantum wells, are compact sources of terahertz (THz) radiation with current pumping. In which, through band engineering, it is possible to obtain generation frequencies from 1.2 to 6.0 THz.^{1–3} To date, the maximum output power of ~2 W⁴ and operating temperature of $T_{\text{max}} = 261$ K⁵ were achieved in a pulsed operation mode. However, many applications such as astronomy, communications, heterodyne spectroscopy, or dual frequency comb spectroscopy require continuous THz lasers. Continuous operation

of THz QCLs was achieved less than a year after the demonstration of the first pulsed THz QCL.^{6,7} Nowadays, the maximum operating temperature of continuous-wave (CW) THz QCLs is 129 K,^{8,9} and the output power is ~0.3 W,¹⁰ which significantly lags behind the characteristics of pulsed THz QCLs. Note that the maximum operating temperatures were obtained in QCLs with metal-metal waveguides, while the record output power was realized using surface plasmon waveguides with a larger output aperture^{8,9} at the cost of reducing the maximum operating temperatures down to 60–65 K.

One of the options for optimizing CW QCLs, which allows increasing the output power while maintaining high operating

temperature, could be the use of the so-called two-photon design. The idea of creating two-photon lasers, in which the relaxation of electrons between quantum levels with population inversion occurs due to the emission of two photons, was expressed back in the 1960s (see, for example, Ref. 11). Such lasers have an enormous potential for applications in frequency metrology, quantum gyroscopes, quantum cryptography, quantum computing and generation of entangled photon pairs, in addition to many conventional frequency-dependent laser applications.¹² However, to date, the potential of two-photon lasers remains largely unexplored because their experimental implementation is challenging. Their first and only implementation in the optical frequency range using barium atoms dates back to 1992.¹³ A QCL operating on intersubband transitions seems to be an ideal medium for realizing two-photon lasing. The possibilities of engineering the levels of the energy spectrum of the active region of a QCL allow creating designs for which the electron transport through one period of the laser heterostructure is accompanied by the emission of two photons. The design of such a “resonant” two-photon QCL (the energies of both photons are the same) with four quantum wells in a period was proposed in Refs. 12, 14, and 15. In Ref. 14, based on a simplified system of balance equations, it was concluded that the nonlinear gain (at a nonzero photon density in the resonator) for a QCL with a two-photon design is approximately two times higher than for a QCL with a single-photon design. This conclusion is confirmed by the results of numerical calculations of the nonlinear gain for the single-photon QCL with three QWs in the period (from Ref. 16) and the two-photon QCL with four QWs in the period,²¹ which should ensure higher generation efficiency in the latter case while maintaining a sufficiently high maximum operating temperature $T \sim 180$ K¹⁵ (cf. Ref. 16). Earlier, in Refs. 17 and 18 (Although not

stated directly, in Ref. 17, a five-level resonant two-photon QCL design with four quantum wells in the period was used.), we demonstrated pulsed two-photon THz QCLs with both “resonant” and “non-resonant” (the energies of the two photons are different) designs. It is also worth mentioning Ref. 19, in which lasing was demonstrated on transitions between two pairs of levels in a terahertz QCL with four quantum wells in a period. In the present paper, a continuous-wave THz QCL with a “non-resonant” two-photon design is developed and demonstrated.

II. DESIGNING QCL HETEROSTRUCTURES

To design the GaAs/Al_xGa_{1-x}As heterostructures of a two-photon QCL, a five-level laser scheme with resonant-phonon depletion of the lower laser level with four quantum wells (QWs) in a period was chosen (see, for example, Refs. 12, 14, and 15). Calculations of the electron transport, the amplification spectra, and the gain were carried out on the basis of a system of balance equations for localized and continuum states. A specially developed method was used to modify the intrinsic basis of the Schrödinger equation by reducing the dipole moments of tunnel-bound states to take into account the influence of dephasing on the charge carrier transport.²⁰ In order to find the design of a heterostructure with a low threshold current and high efficiency, two-photon designs with four quantum wells in the period of the active region were optimized by scanning the thicknesses of GaAs QWs and Al_{0.15}Ga_{0.85}As barrier layers. Figure 1(a) shows the conduction band diagrams, the energy levels, and the moduli squares of wave functions of an optimized design at the operating bias with a following sequence of layers: **5.64/16.38/7.34/8.47/4.23/9.03/3.39/9.03** nm (Al_{0.15}Ga_{0.85}As barriers are indicated in bold).

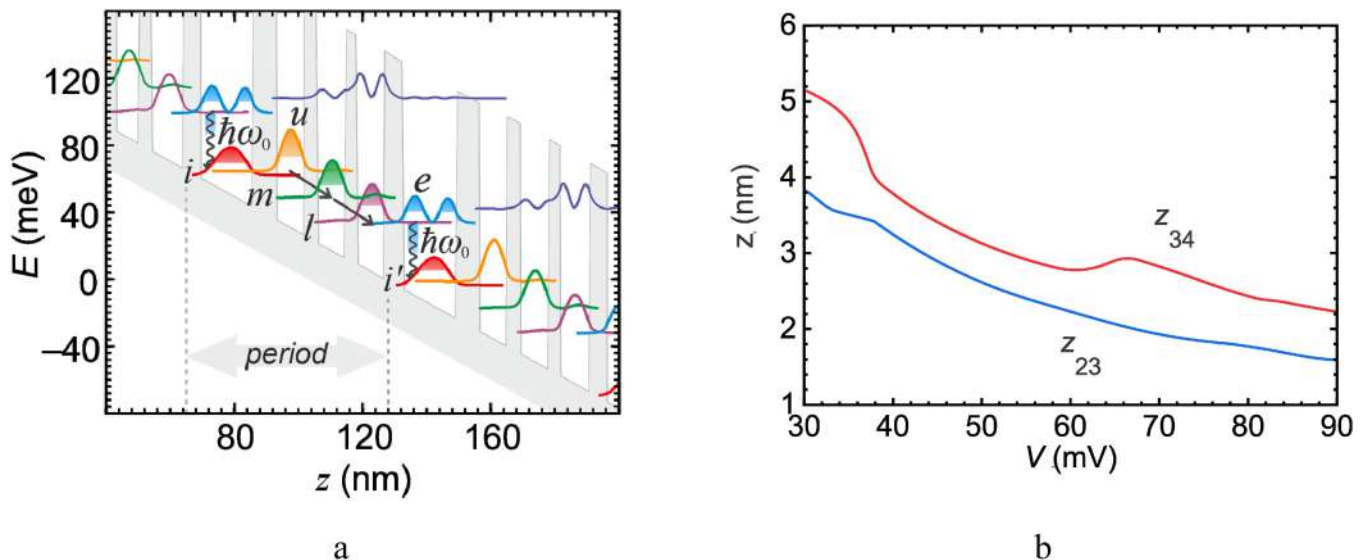


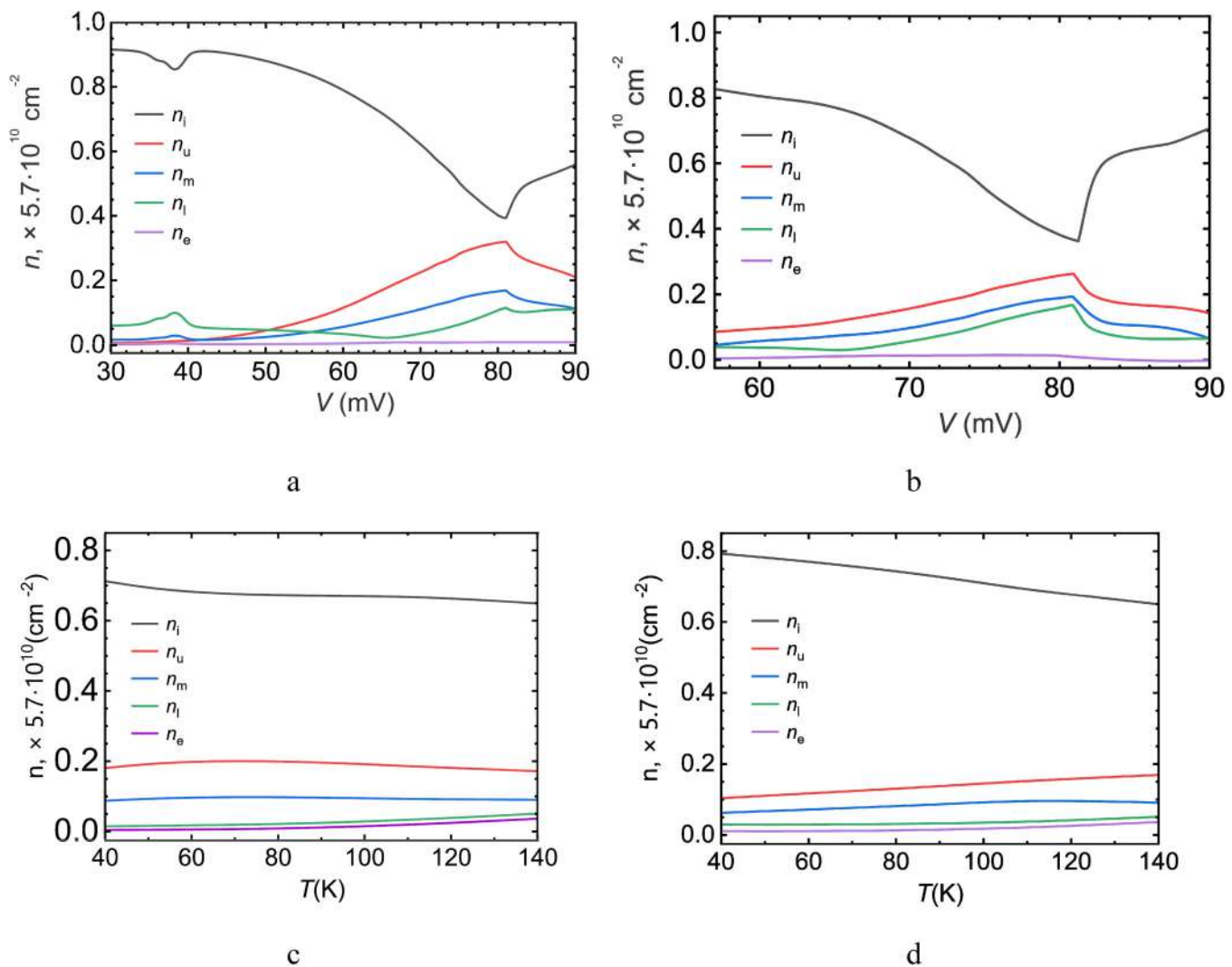
FIG. 1. (a) Conduction band diagram and squared moduli of electron wave functions, calculated by the k-p method, for the optimized structure of a THz QCL based on GaAs/Al_{0.15}Ga_{0.85}As at a temperature $T = 70$ K and a voltage across the structure period $V = 66$ mV. Arrows indicate radiative transitions. The dashed rectangle marks the period of the cascade structure. (b) Dependences of matrix elements for radiative transitions z_{u-m} (z_{23}) and z_{m-l} (z_{34}) on the applied voltage at the structure period V .

24 February 2025 16:15:49

The central part of the wide QW was doped with a donor impurity with a layer concentration of $5.7 \times 10^{10} \text{ cm}^{-2}$. The reduction in heat release at the operating voltage, which is necessary to implement the continuous operating mode of the QCL, is achieved by the means of the record-wide (for known THz QCL designs) injection barrier of 7.34 nm (and a corresponding decrease in the tunneling current). In each period of the structure, the electron transport and the operational optical transitions occur through the following levels: injector (i), upper (u), middle (m), lower (l) laser levels, and extractor level (e). For efficient electron transfer, the injector level i is tunnel coupled to the upper laser level u . The lower laser level l is tunnel coupled to the extractor level e , which, for effective depletion, is spaced from

the injector level i' of the next period by the energy of the longitudinal optical phonon. Figure 1(b) shows the dependences of matrix elements on the voltage across the structure period for both radiative transitions.

The dependences of the populations of QCL levels on voltage and temperature are shown in Fig. 2 for the modes with and without lasing. The population of the u level is always greater than the population of the m level, and the population of the m level is always greater than the population of the l level, i.e., the population inversion takes place. With increasing voltage (up to 80 mV), the populations of the laser levels increase, and the population of the injector level decreases. Calculations show that the lasing is possible up to a temperature of 140 K [Fig. 2(d)].



24 February 2025 16:15:49

FIG. 2. Populations of the QCL working levels vs the voltage at the structure period at $T = 70 \text{ K}$ (a) and (b) and on the temperature at $V = 66 \text{ mV}$ (c) and (d) in the linear (a) and (c) and nonlinear [(b) and (d), in the lasing regime] modes.

The required gain at a low threshold current within the proposed design is achieved by reducing the spectral broadening of laser transitions $u \rightarrow m$ and $m \rightarrow l$. The broadening arises due to the influence of non-radiative transitions during tunneling, scattering by phonons, impurities, and heterointerface roughness. For laser levels u and m , the total calculated broadening is 0.53 meV, which is achieved through the use of thick barriers and selective doping. At the same time, the probability of a transition between levels i and u , through the widest injection barrier of 7.34 nm at an operating bias of 66 mV per period is $5.8 \times 10^{10} \text{ s}^{-1}$, and is mainly caused by the scattering processes on impurities and heterointerface roughness. Calculations were performed for the root-mean-square fluctuation of the thickness of layers of 0.38 nm and the correlation length between irregularities in the plane of a layer of 9 nm (cf. Ref. 21). A wide (4.23 nm) barrier between the laser levels u and m ensures a low probability of non-radiative $u \rightarrow m$ transition ($\sim 9.5 \times 10^{10} \text{ s}^{-1}$), which is necessary to maintain the population inversion keeping a moderate probability of depletion of the middle laser level ($\sim 1.9 \times 10^{11} \text{ s}^{-1}$). The lower laser level l is depopulated by resonant tunneling ($\sim 1.6 \times 10^{12} \text{ s}^{-1}$) to the extractor e , which is connected to the injector of the next period via the emission of optical phonons ($\sim 4.0 \times 10^{12} \text{ s}^{-1}$). In this case, the populations of the levels i , u , m , and l are 68, 20, 9.8, and 1.9 percent of the total electron concentration, respectively. Diagonal matrix elements of laser transitions $Z_{u-m} = 2 \text{ nm}$ and $Z_{m-l} = 3 \text{ nm}$ (at $V = 66 \text{ mV}$) are sufficient to overcome the total losses of $\sim 13 \text{ cm}^{-1}$. Figure 3(a) shows the gain spectra calculated in a one-dimensional approximation in linear and nonlinear (under lasing conditions) regimes at different bias values, as well as the loss spectrum of a metal-metal waveguide. With increasing the bias, the amplification

first occurs at the upper $u \rightarrow m$ transition, and the second $m \rightarrow l$ transition joins at a further bias increase and the gain spectrum becomes “double-humped” covering the spectral range of 3.4–4.3 THz. Figure 3(b) shows the calculated values of the linear gain at the maximum (over the spectrum) at various values of bias per structure period and waveguide losses as a function of the temperature. It can be seen that the maximum operating temperatures (when the gain equals to the losses) lie in the range of 120–140 K. For the CW mode, the lattice temperature can be 15–45 K higher than the temperature of the heat sink.²²

III. MBE GROWTH AND QCL PROCESSING

The QCL heterostructure was grown by molecular beam epitaxy (MBE), which is currently the base technology for manufacturing infrared (IR) and THz QCLs in various material systems.^{23,24} Epitaxial growth of QCL heterostructures with a large number of layers requires precision control of individual layers with characteristic thicknesses of several nanometers, their composition, the repetition period of individual fragments of the active region, the level of doping of the active region, and ensuring a low level of background doping.^{25,26} As applied to THz QCL structures, the task is complicated by their large total thickness ($\sim 10 \mu\text{m}$), which places increased demands on the stability of the parameters of the epitaxial process for 10–15 h.

In this work, a single-substrate Riber C21 research-grade MBE setup was used to grow THz QCL heterostructures in the AlGaAs/GaAs system. The growth of laser heterostructures was preceded by careful calibration using high-resolution x-ray diffractometry for a set of grown AlGaAs/GaAs superlattices with

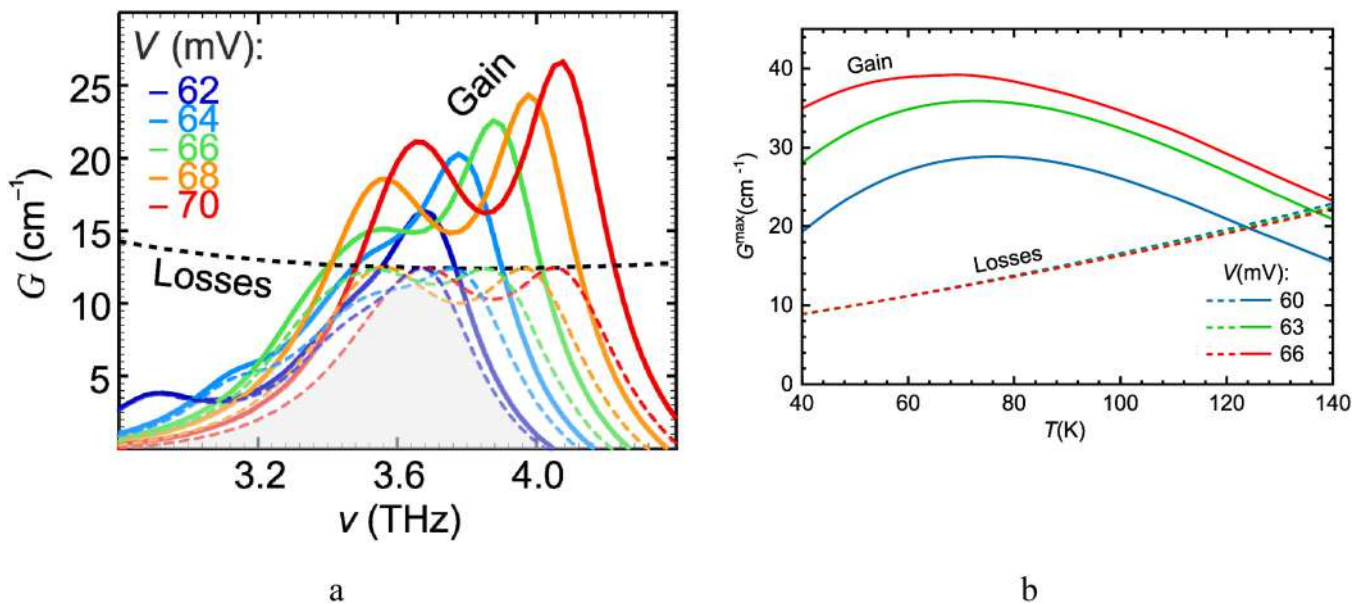


FIG. 3. (a) Spectra of linear (solid lines) and nonlinear (in the lasing regime, dashed lines) gain and loss for various voltages at the structure period V at $T = 70 \text{ K}$. (b) Temperature dependences of the maximum gain (solid curves) for various voltages at the structure period V and total losses (dashed curves).

parameters close to individual fragments of the QCL active region. This is fundamentally necessary due to the transient effects inherent in the MBE method when the shutters of molecular sources are activated.²⁷ To analyze the quality of the grown epitaxial structures, the surface density of defects was measured. The characteristic density of surface defects with an area greater than $1\mu\text{m}^2$ for the fabricated QCL heterostructures, measured using laser radiation scattering analysis, was 500–600 defects/cm². Despite the rather high probability, for a given surface density of defects, of one or more defects falling within the stripe structure of manufactured lasers, this does not lead to significant shunt conductivity. To precisely calibrate the doping of GaAs layers with a silicon donor impurity, a capacitance–voltage profiling technique was used, which ensures an absolute accuracy of control of the doping level of $\sim 2.5\%$.²⁸

The THz QCL heterostructure was grown on a semi-insulating GaAs substrate with a crystallographic orientation (001) with a diameter of 76 mm. The characteristic growth rates of the layers were 1.25–2 Å/s, the substrate temperature was about 580 °C. During the growth, the temperature of the Ga molecular source was gradually adjusted (a linear increase of 0.3 °C during the growth of the active region) to compensate for its depletion. It is known that such an adjustment during a long epitaxial process is fundamentally important for a Ga source, while the value of the atomic flux from an Al source during the growth of QCL structures usually remains quite stable.

The growth of the THz QCL heterostructure was preceded by the fabrication of a test superlattice containing 35 pairs of $\text{Al}_{0.15}\text{Ga}_{0.85}\text{As}/\text{GaAs}$ layers. A similar test superlattice was grown after the fabrication of the THz QCL heterostructure. Figure 4 shows high-resolution x-ray diffraction patterns measured for two fabricated test superlattices. According to the results of their analysis, the thicknesses of the AlGaAs and GaAs layers for the first superlattice are 62.6 and 69 Å, respectively, and for the second—62 and 69.4 Å. The good agreement between the measured parameters

of the superlattices confirms the high stability of the epitaxial process during the growth of the THz QCL heterostructure. Then, a chip with ridge mesa stripes with double metal (gold) waveguide (DMW) was fabricated. The procedure for producing QCL ridges with DMW is described in detail in Refs. 29 and 30. Distinctive manufacturing features were narrow (20 and 30 μm wide) laser ridges that make it possible to reduce the QCL operation currents, compared to standard 100 μm wide ridges. In addition, to reduce the absorption of THz radiation by free carriers, precision liquid etching of the upper n^+ -GaAs contact layer to a thickness of about 70 nm was carried out. After all operations for the processing of DMW, the back side of the chip substrate was subjected to chemical–mechanical polishing to decrease the thickness of the substrate down to 120 μm . Next, Ti/Pd/Au metallization was sputtered onto the back side of the substrate for assembly on a copper heat sink.

The fabricated chip with DMW ridges was cleaved into pieces containing 2.9 mm long and 20 and 30 μm wide QCL ridges. These “microchips” were then soldered onto copper heat sinks (C-mount) using indium solder. Gold wires with a diameter of 18 μm were welded to the ridges using the “ball-wedge” thermosonic microwelding method—Fig. 5. There were at least six wires per ridge, located at approximately equal intervals along the length of the ridges, for uniform injection of current into the active region of the QCL.

IV. EXPERIMENTAL

The studies of the current–voltage (V – I) characteristics and the dependences of the integral radiation intensity on the pump current (L – I characteristics) of the fabricated THz QCLs with a double metal waveguide were carried out at different temperatures in both pulsed and continuous modes. The lasers were mounted on a cold finger in a closed-cycle optical cryostat. All the results presented below in the figures were obtained for the QCL sample 82117L (ridge width of 30 μm) placed in a CFA-201 cryostat

24 February 2025 16:15:49

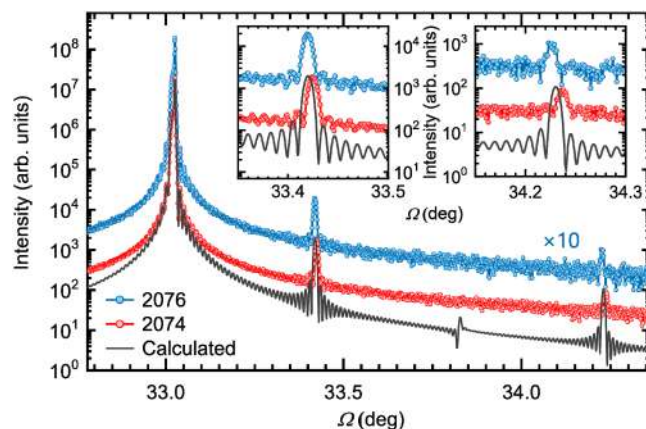


FIG. 4. High-resolution x-ray diffraction patterns measured for two nominally identical test superlattices fabricated immediately before (2074, red symbols) and after (2076, blue symbols) growth of the THz QCL heterostructure and the calculated HR XRD pattern (black curve).

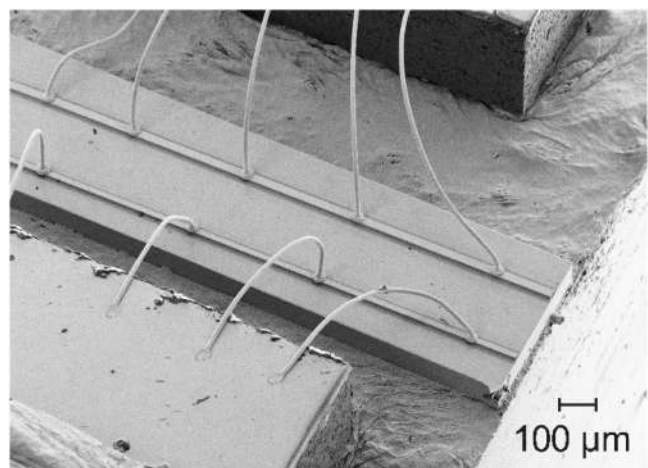


FIG. 5. Scanning electron microscope image of two laser ridges 20 and 30 μm wide, welded with a gold wire with a diameter of 18 μm .

(Cryogenic Instruments LLC, Moscow) with a minimum operating temperature of 8 K and a cooling capacity of 7.5 W at 20 K. Windows made of polymethylpentene (TPX) were used to output radiation. To power the QCL in a pulsed mode, specially made electronic switches were used, which made it possible to generate pulses of specified duration, duty cycle and amplitude, as well as to measure the voltage and current passing through the laser. When operating in a continuous mode, the QCL was powered by a Keithley 2400 source-meter, which made it possible to simultaneously measure the output voltage and current and provide their continuous sweep. When recording L - I characteristics, the QCL radiation was collimated by a TPX lens placed directly at the cleaved edge of the laser ridge, modulated by a chopper with a frequency of 12 Hz, and recorded by a THZ51-BL-BNC pyroelectric detector (Gentec Electro-Optics, Inc.). The signal from the detector was digitized by a Tektronix TDS3034B oscilloscope and recorded in the computer memory as a function of the laser current. The emission spectra were recorded using a BRUKER Vertex 80v evacuated Fourier-transform spectrometer, operating in the fast scanning mode when recording emission spectra of CW QCL and in the step-scan mode when recording QCL spectra in a pulse mode. The spectral resolution was 0.1 cm^{-1} . The standard pyroelectric detector of the spectrometer (when the QCL is operating in a CW mode) and a Ge:Ga photodetector placed in a light guide insert in a storage liquid helium Dewar vessel (for both modes) were used as radiation detectors. During spectral studies, QCL radiation was focused onto the entrance window of the Fourier-transform spectrometer using two off-axis parabolic mirrors.

V. RESULTS AND DISCUSSION

Figure 6 shows the measured current-voltage and L - I characteristics of QCL 82117L (ridge width of $30 \mu\text{m}$), operating in a

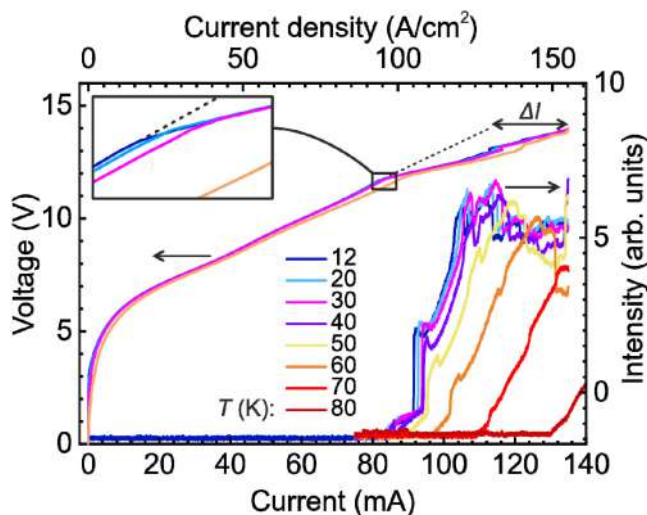


FIG. 6. V - I and L - I characteristics of QCL 82117L in the CW mode at different temperatures.

continuous mode, at various temperatures. The maximum operating temperatures of this laser were ~ 90 and ~ 95 K in the CW and in the pulsed (pulse duration less than $1 \mu\text{s}$) mode, respectively. The laser with the ridge width of $20 \mu\text{m}$ demonstrates nearly the same temperature behavior. Such a slight difference in operating temperatures contrasts with the literature data, which report the difference in maximum temperatures in continuous and pulsed modes is tens of Kelvin (see, for example, Refs. 7–9). This indicates that in the studied structure, the overheating of the active region of the laser in continuous mode is small and the maximum operating temperatures in both cases are determined by the condition of equality of gain and losses. These values are somewhat smaller than the calculated values [see Fig. 3(b)], which was to be expected, taking into account the limitations of the one-dimensional model (which does not take into account the losses at the boundaries of the waveguide of finite width).

As can be seen in Fig. 6, the current-voltage characteristics exhibit characteristic features (kinks) corresponding to the QCL threshold currents, which shift to higher currents with increasing temperature. The kink in the current-voltage characteristic, corresponding to a decrease in the differential resistance of the device, is observed only in fairly “good” QCLs and is associated with the inclusion of the “photonic” mechanism of electron transport (cf. Ref. 31). Based on the expression of slope efficiency from Ref. 10, one can estimate the output optical power (from both facets),

$$P_{\text{opt}} = 2N \frac{\Delta I}{e} \frac{\alpha_m}{\alpha_m + \alpha_w} \hbar \omega. \quad (1)$$

Here the factor 2 stands for two photons emitted at each period of the QCL heterostructure, $N=157$ is the number of periods, $\Delta I=24 \text{ mA}$ is the value of the “additional” current (see Fig. 6), e is the elementary charge, $\alpha_m = (1/2L)\ln(1/r^2)$ is the mirror loss ($L=0.288 \text{ cm}$ is the waveguide length, r is the facet reflectivity), $\alpha_w = 13 \text{ cm}^{-1}$ is the waveguide loss [see Fig. 3(b)] and $\hbar \omega \approx 13.5 \text{ meV}$ is the “average” energy of emitted photons (determined from the emission spectra). For the metal-metal waveguide, the facet reflectivity is rather high and can be estimated as $r \approx 0.85$ for a waveguide cross section of $30 \times 10 \mu\text{m}^2$ (see Fig. 13 in Ref. 32). Substituting the above values into (1), one obtains $P_{\text{opt}} \approx 4.3 \text{ mW}$. The actually recorded output optical power turns out to be significantly lower due to the complex structure of the radiation wavefront, which prevents its collimation.³³

L - I characteristics, presented in Fig. 6, demonstrate numerous features that generally shift toward higher currents with increasing temperature. The maximum radiation intensity corresponds to a certain applied voltage, which determines the relative position of the QCL working levels. As can be seen in Fig. 6, with increasing temperature, this voltage value is achieved at a higher current value, which also leads to a corresponding shift in the position of the maximum radiation intensity. Therefore, the radiation intensity at the maximum at a higher temperature may exceed the radiation intensity below the maximum at a lower temperature, as shown in Fig. 6. Sharp changes in the radiation intensity (both increase and decrease) during current sweep are obviously associated with changes in the mode composition of the QCL emission spectra. In this regard, it is worth comparing the

24 February 2025 16:15:49

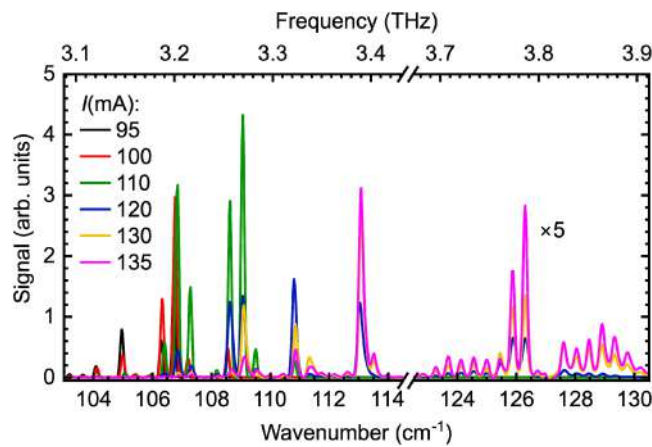


FIG. 7. CW emission spectra of QCL 82117L at various currents: $T = 12$ K.

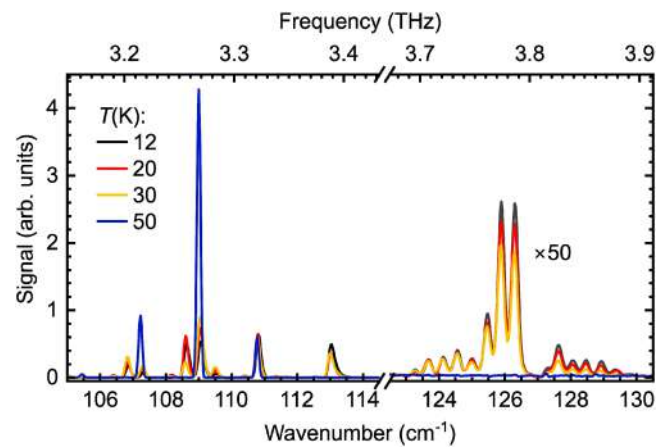
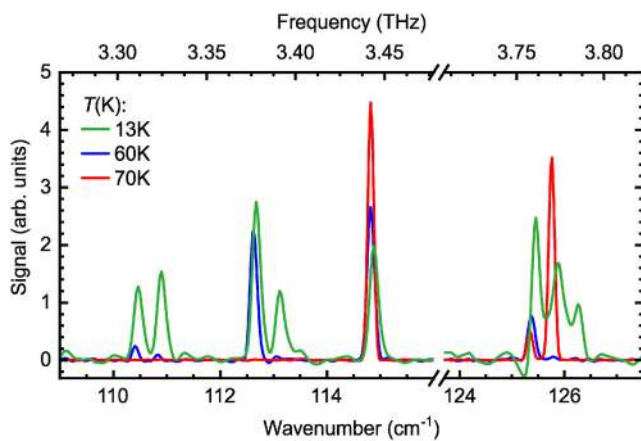


FIG. 8. Emission spectra of QCL 82117L in the CW mode at various temperatures and a current of 120 mA.

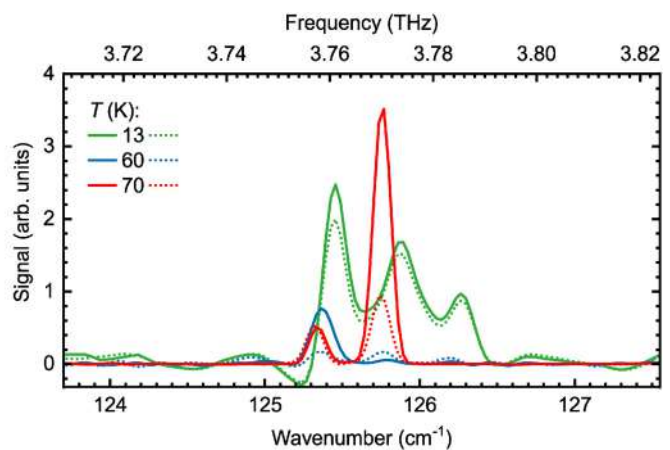
spectra measured at different points of the L - I curve—Fig. 7. At a current of 95 mA, lasing occurs in the low-frequency region of 103 – 105 cm^{-1} and as the current increases to 110 mA, progressively more higher-frequency modes are “ignited” up to 113 cm^{-1} , that is natural for the QCL design with “diagonal” transitions, when the energy separation between upper and lower laser levels increases with the bias. Finally, at currents of 120 – 135 mA, an additional high-frequency lasing band appears in the region of 123 – 130 cm^{-1} . At the same time, no lasing is observed in between 114 and 123 cm^{-1} . Thus, the emission spectrum is dual-band that corresponds to the design of a “non-resonant” two-photon laser [see Fig. 3(a)]. However, the low-frequency band, which, judging

by the design, corresponds to the m - l transition [see Fig. 1(a)], “ignites” first with the bias increase, while according to the calculation, lasing should initially occur at the u - m transition [Fig. 3(a)]. Most likely, the population inversion between the upper (u) and the middle (m) levels is less than the calculated one. Unlike the lower laser level (l), which is depleted due to the resonant scattering of optical phonons, there is no such effective mechanism of depopulation for the middle level. The model used for calculations²⁰ does not take into account, in particular, the effective electron temperature, which is obviously higher than the lattice temperature. The observed emission frequencies also

24 February 2025 16:15:49



a



b

FIG. 9. (a) Emission spectra of QCL 82117L in the pulsed mode ($\tau = 100$ μs , $f_{\text{rep}} = 1$ kHz) at $T = 13$ – 70 K and a current of 120 mA. The signal was sampled at the beginning of the pulse. (b) Emission spectra in the high-frequency lasing band at $T = 13$ – 70 K and a current of 120 mA when sampling the signal at the beginning (solid lines) and at the end (dashed lines) of the pulse.

turned out to be lower than the calculated ones, which indicate the limited applicability of the model used.

Figure 8 shows the emission spectra of the QCL 82117L at a fixed current of 120 mA and various temperatures of 12–50 K. It can be seen that the increase in temperature to 30 K has little effect on the emission spectrum, but already at 50 K, the high-frequency lasing band disappears and the low-frequency band is noticeably narrowed. In this case, the intensity of the mode at 109.0 cm^{-1} sharply increases, while the integral intensity remains practically unchanged—see Fig. 6. Figure 9 shows the QCL emission spectra measured in a pulsed mode at different temperatures at the same current of 120 mA. The pulse duration and the repetition rate were $100\text{ }\mu\text{s}$ and 1 kHz, respectively. The spectra in Fig. 9(a) were recorded when the signal was sampled at the beginning of the pulse. It can be seen that in this case the high-frequency band remains comparable in intensity to the low-frequency one even at a temperature of 70 K. Sampling of the signal at the end of a 100-microsecond pulse shows that the intensities of the emission lines in the low-frequency band of $110\text{--}115\text{ cm}^{-1}$ change little compared with those at the beginning of the pulse. At the same time, in the high-frequency emission band of $125\text{--}126.5\text{ cm}^{-1}$ at temperatures of 60 and 70 K, the intensities of the emission lines decrease by 3–4 times during $100\text{ }\mu\text{s}$ pulse—Fig. 9(b). Since the high-frequency band is associated with transitions from the upper u to the middle laser level m , this indicates that in the continuous lasing mode, the population of the m level increases with increasing temperature, which leads to a decrease in the population inversion at the $u\text{--}m$ transition. The same thing happens due to heating of the active region of the QCL during a long current pulse.

Figure 10 demonstrates the possibility of QCL frequency tuning by changing either temperature or current. At a constant current of 120 mA, the emission line of the QCL 82117L exhibits “red” shift (decrease in mode frequency) with temperature changes in the range of 12–65 K, amounting to about -0.2 cm^{-1} (-6 GHz), resulted from an increase in the effective refractive index of the

waveguide due to heating of the crystal lattice (see, for example, Refs. 34–36)—Fig. 10(a). The opposite “blue” shift (increase in mode frequency) is observed with increasing current [see Fig. 10(b)], which is due to the effect of “pulling” of modes when the gain profile is tuned by the bias, resulting in the corresponding change in the real part of the dielectric constant (and, accordingly, the effective refractive index) of the waveguide according to the Kramers–Kronig relations. For QCLs with diagonal optical transitions, an increase in the current and, accordingly, the voltage across the structure leads to a shift of the gain spectrum to the short-wavelength region, which makes a negative contribution to the refractive index at lower frequencies (see, for example, Refs. 37–39). As can be seen from Fig. 10(b), the magnitude of the mode frequency shift reaches $+0.15\text{ cm}^{-1}$ ($+4.5\text{ GHz}$). Thus, for the 82117L QCL under study, it is possible to achieve a total tuning of the emission line by $\sim 10\text{ GHz}$ by changing the current and temperature.

VI. CONCLUSIONS

To conclude, the work demonstrates for the first time a continuous-wave THz QCL with a “non-resonant” two-photon design, in which two-band emission is realized. The maximum operating temperature is about 90 K, which allows the device to be operated using simple single-stage closed-cycle cryostats. The possibility of tuning the frequency of the radiation mode with temperature and operating current has been demonstrated, which opens up the prospect of using the device for spectroscopic applications.

ACKNOWLEDGMENTS

The work was supported by the Russian Science Foundation Grant No. 23-19-00436. The growth of the QCL heterostructure was carried out within the framework of the Russian Science Foundation Project No. 21-72-30020. A.A.D. and V.A.A. were supported by the state assignment of Ministry of Science and Higher Education of the Russian Federation FFUF-2024-0045. D.A.B. is grateful to the Theoretical Physics and Mathematics Advancement Foundation “BASIS” scholarship for the support. The authors are grateful to M.A. Fadeev for assistance with measurements and useful discussions.

AUTHOR DECLARATIONS

Conflict of Interest

The authors have no conflicts to disclose.

Author Contributions

R. A. Khabibullin: Conceptualization (equal); Investigation (equal); Methodology (equal); Project administration (equal); Resources (equal); Supervision (equal); Writing – review & editing (equal). **D. V. Ushakov:** Conceptualization (equal); Investigation (equal); Methodology (equal); Writing – original draft (equal). **A. A. Afonenko:** Conceptualization (equal); Investigation (equal); Methodology (equal); Writing – original draft (equal). **A. Yu. Pavlov:** Investigation (equal); Methodology (equal). **R. R. Galiev:** Investigation (equal); Methodology (equal).

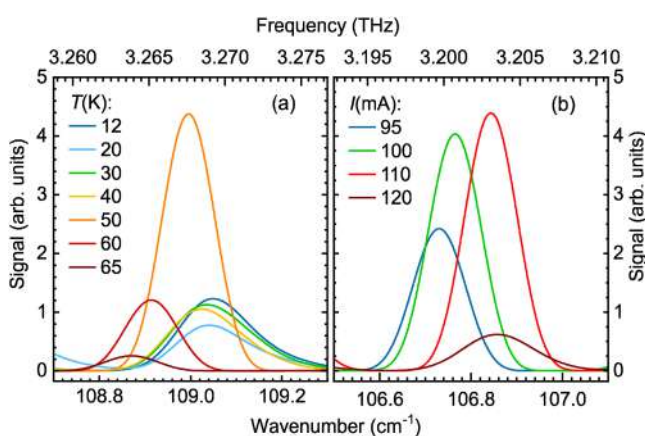


FIG. 10. Frequency tuning of the CW QCL 82117L with increasing (a) temperature ($I = 120\text{ mA}$, pyroelectric detector) and (b) current ($T = 12\text{ K}$, Ge:Ga photodetector).

D. S. Ponomarev: Conceptualization (equal); Investigation (equal); Methodology (equal). **A. P. Vasilyev:** Investigation (equal); Methodology (equal). **A. G. Kuzmenkov:** Investigation (equal); Methodology (equal). **N. A. Maleev:** Conceptualization (equal); Investigation (equal); Methodology (equal); Resources (equal); Validation (equal); Writing – original draft (equal). **F. I. Zubov:** Investigation (equal); Methodology (equal); Resources (equal). **M. V. Maksimov:** Investigation (equal); Methodology (equal). **D. A. Belov:** Investigation (equal); Methodology (equal). **A. V. Ikonnikov:** Investigation (equal); Methodology (equal); Resources (equal); Writing – review & editing (equal). **D. I. Kuritsyn:** Investigation (equal); Methodology (equal). **R. Kh. Zhukavin:** Investigation (equal); Methodology (equal). **K. A. Kovalevsky:** Investigation (equal); Writing – original draft (equal). **V. A. Anfertev:** Investigation (equal); Methodology (equal). **V. L. Vaks:** Investigation (supporting); Validation (equal). **A. V. Antonov:** Investigation (supporting); Methodology (equal); Resources (equal). **A. A. Dubinov:** Conceptualization (equal); Funding acquisition (equal). **S. V. Morozov:** Investigation (supporting); Validation (equal). **V. I. Gavrilenko:** Conceptualization (equal); Investigation (equal); Methodology (equal); Project administration (equal); Resources (equal); Supervision (equal); Writing – original draft (equal).

DATA AVAILABILITY

The data that support the findings of this study are available from the corresponding author upon reasonable request.

REFERENCES

- ¹M. S. Vitiello, G. Scalari, B. Williams, and P. De Natale, “Quantum cascade lasers: 20 years of challenges,” *Opt. Express* **23**, 5167 (2015).
- ²G. Liang, T. Liu, and Q. J. Wang, “Recent developments of terahertz quantum cascade lasers,” *IEEE J. Sel. Top. Quant. Electron.* **23**, 1200118 (2017).
- ³M. Shahili, S. J. Addamane, A. D. Kim, C. A. Curwen, J. H. Kawamura, and B. S. Williams, “Continuous-wave GaAs/AlGaAs quantum cascade laser at 5.7 THz,” *Nanophotonics* **13**, 1735 (2024).
- ⁴L. H. Li, L. Chen, J. R. Freeman, M. Salih, P. Dean, A. G. Davies, and E. H. Linfield, “Multi-watt high-power THz frequency quantum cascade lasers,” *Electron. Lett.* **53**, 799 (2017).
- ⁵A. Khalatpour, M. C. Tam, S. J. Addamane, J. Reno, Z. Wasilewski, and Q. Hu, “Enhanced operating temperature in terahertz quantum cascade lasers based on direct phonon depopulation,” *Appl. Phys. Lett.* **122**, 161101 (2023).
- ⁶L. Ajili, G. Scalari, D. Hofstetter, M. Beck, J. Faist, H. Beere, G. Davies, E. Linfield, and D. Ritchie, “Continuous-wave operation of far-infrared quantum cascade lasers,” *Electron. Lett.* **38**, 1675 (2002).
- ⁷S. Barbieri, J. Alton, S. S. Dhillon, H. E. Beere, M. Evans, E. H. Linfield, A. G. Davies, D. A. Ritchie, R. Kohler, A. Tredicucci, and F. Beltram, “Continuous-wave operation of terahertz quantum-cascade lasers,” *IEEE J. Quantum Electron.* **39**, 586 (2003).
- ⁸M. Wienold, B. Röben, L. Schrottke, R. Sharma, A. Tahaoui, K. Biermann, and H. T. Grah, “High-temperature, continuous-wave operation of terahertz quantum-cascade lasers with metal-metal waveguides and third-order distributed feedback,” *Opt. Express* **22**, 3334 (2014).
- ⁹C. A. Curwen, S. J. Addamane, J. L. Reno, M. Shahili, J. H. Kawamura, R. M. Briggs, B. S. Karasik, and B. S. Williams, “Thin THz QCL active regions for improved continuous-wave operating temperature,” *AIP Adv.* **11**, 125018 (2021).
- ¹⁰W. Li, Y. Li, Y. Ma, Y. Xu, J. Liu, N. Zhuo, Q. Lu, L. Wang, J. Zhang, S. Zhai, S. Liu, and F. Liu, “Continuous-wave terahertz quantum cascade laser based on a hybrid bound to bound quantum design,” *Front. Photonics* **3**, 1071879 (2022).
- ¹¹A. M. Prokhorov, “Quantum electronics,” *Science* **149**, 828 (1965).
- ¹²M. A. Talukder, P. Dean, E. H. Linfield, and A. G. Davies, “Resonant two-photon terahertz quantum cascade laser,” *Opt. Express* **30**, 31785 (2022).
- ¹³D. J. Gauthier, Q. Wu, S. E. Morin, and T. W. Mossberg, “Realization of a continuous-wave, two-photon optical laser,” *Phys. Rev. Lett.* **68**, 464 (1992).
- ¹⁴D. V. Ushakov, A. A. Afonenko, R. A. Khabibullin, V. K. Kononenko, and I. S. Manak, “Gain saturation effects in THz quantum cascade lasers,” *Proc. Nat. Acad. Sci. Belarus* **58**, 237 (2022).
- ¹⁵D. V. Ushakov, A. A. Afonenko, D. S. Ponomarev, S. S. Pushkarev, V. I. Gavrilenko, and R. A. Khabibullin, “New designs of laser transitions in terahertz quantum-cascade lasers,” *Radiophys. Quantum Electron.* **65**, 461 (2022).
- ¹⁶S. Kumar, Q. Hu, and J. L. Reno, “186 K operation of terahertz quantum-cascade lasers based on a diagonal design,” *Appl. Phys. Lett.* **94**, 131105 (2009).
- ¹⁷T. A. Bagaev, M. A. Ladugin, A. A. Marmalyuk, A. I. Danilov, D. V. Ushakov, A. A. Afonenko, A. A. Zaytsev, K. V. Maremyanin, S. V. Morozov, V. I. Gavrilenko, R. R. Galiev, A. Y. Pavlov, S. S. Pushkarev, D. S. Ponomarev, and R. A. Khabibullin, “3.8 THz quantum cascade laser grown by metalorganic vapor phase epitaxy,” *Tech. Phys. Lett.* **48**(5), 46 (2022).
- ¹⁸V. I. Gavrilenko, “Two-photon THz quantum cascade lasers,” in *Proceedings of Russian Conference on Actual Problems of Semiconductors and Photoelectronics (Photonics 2023), September 4–8, 2023, Novosibirsk (Pero, 2023)*, p. 26, see <https://www.isp.nsc.ru/upload/photonics2023/photonics2023.pdf>. ISBN: 978-5-00218-581-8.
- ¹⁹B. Wen, C. Xu, S. Wang, K. Wang, M. C. Tam, Z. Wasilewski, and D. Ban, “Dual-lasing channel quantum cascade laser based on scattering-assisted injection design,” *Opt. Express* **26**, 9194 (2018).
- ²⁰D. V. Ushakov, A. A. Afonenko, A. A. Dubinov, V. I. Gavrilenko, O. Y. Volkov, N. V. Shchavruk, D. S. Ponomarev, and R. A. Khabibullin, “Balance-equation method for simulating terahertz quantum-cascade lasers using a wave-function basis with reduced dipole moments of tunnel-coupled states,” *Quantum Electron.* **49**, 913 (2019).
- ²¹K. Leosson, J. R. Jensen, W. Langbein, and J. M. Hvam, “Exciton localization and interface roughness in growth-interrupted GaAs/AlAs quantum wells,” *Phys. Rev. B* **61**, 10322 (2000).
- ²²W. Freeman, “Double longitudinal-optical phonon intrawell depopulated terahertz quantum cascade structures: Electron transport modeling using a density matrix method,” *Appl. Phys. Lett.* **118**, 241107 (2021).
- ²³J. Faist, F. Capasso, D. L. Sivco, C. Sirtori, A. L. Hutchinson, and A. Y. Cho, “Quantum cascade laser,” *Science* **264**, 553 (1994).
- ²⁴C. Gmachl, F. Capasso, D. L. Sivco, and A. Y. Cho, “Recent progress in quantum cascade lasers and applications,” *Rep. Prog. Phys.* **64**, 1533 (2001).
- ²⁵L. H. Li, J. X. Zhu, L. Chen, A. G. Davies, and E. H. Linfield, “The MBE growth and optimization of high performance terahertz frequency quantum cascade lasers,” *Opt. Express* **23**, 2720 (2015).
- ²⁶N. Stanojević, A. Dmić, N. Vuković, P. Dean, Z. Ikonić, D. Indjin, and J. Radovanović, “Effects of background doping, interdiffusion and layer thickness fluctuation on the transport characteristics of THz quantum cascade lasers,” *Sci. Rep.* **14**, 5641 (2024).
- ²⁷S. Gozu, T. Mozume, H. Kuwatsuka, and H. Ishikawa, “Effects of shutter transients in molecular beam epitaxy,” *Nanoscale Res. Lett.* **7**, 620 (2012).
- ²⁸D. V. Mokhov, T. N. Berezovskaya, A. G. Kuzmenkov, N. A. Maleev, S. N. Timoshnev, and V. M. Ustinov, “Precision calibration of the silicon doping level in gallium arsenide epitaxial layers,” *Tech. Phys. Lett.* **43**, 909 (2017).
- ²⁹R. A. Khabibullin, N. V. Shchavruk, D. S. Ponomarev, D. V. Ushakov, A. A. Afonenko, I. S. Vasil’evskii, A. A. Zaycev, A. I. Danilov, O. Y. Volkov, V. V. Pavlovskiy, K. V. Maremyanin, and V. I. Gavrilenko, “Temperature dependences of the threshold current and output power of a quantum-cascade laser emitting at 3.3 THz,” *Semiconductors* **52**, 1380 (2018).
- ³⁰R. A. Khabibullin, N. V. Shchavruk, D. S. Ponomarev, D. V. Ushakov, A. A. Afonenko, K. V. Maremyanin, O. Y. Volkov, V. V. Pavlovskiy, and

A. A. Dubinov, "The operation of THz quantum cascade laser in the region of negative differential resistance," *Opto-Electron. Rev.* **27**, 329 (2019).

³¹R. Sharma, L. Schrottke, M. Wienold, K. Biermann, R. Hey, and H. T. Grahn, "Effect of stimulated emission on the transport characteristics of terahertz quantum-cascade lasers," *Appl. Phys. Lett.* **99**, 151116 (2011).

³²S. Kohen, B. S. Williams, and Q. Hu, "Electromagnetic modeling of terahertz quantum cascade laser waveguides and resonators," *J. Appl. Phys.* **97**, 053106 (2005).

³³E. E. Orlova, P. M. Solyankin, A. A. Angeluts, A. Lee, O. G. Kosareva, I. A. Ozheredov, A. V. Balakin, V. A. Andreeva, N. A. Panov, V. N. Aksenov, and A. P. Shkurinov, "Spatial filtering of radiation from wire lasers," *Laser Phys. Lett.* **14**, 045001 (2017).

³⁴J. M. Hensley, J. Montoya, J. Xu, L. Mahler, A. Tredicucci, H. E. Beere, and D. A. Ritchie, "Spectral behavior of a terahertz quantum cascade laser," *Opt. Express* **17**, 20476 (2009).

³⁵A. A. Lastovkin, A. V. Ikonnikov, V. I. Gavrilenko, A. V. Antonov, and Y. G. Sadof'ev, "Studying the frequency tuning of pulsed terahertz quantum cascade lasers," *Radiophys. Quantum Electron.* **54**, 609 (2012).

³⁶A. A. Lastovkin, A. V. Ikonnikov, A. V. Antonov, V. Y. Aleshkin, V. I. Gavrilenko, and Y. G. Sadof'ev, "Variation of the emission frequency of a terahertz quantum cascade laser," *Tech. Phys. Lett.* **42**, 230 (2016).

³⁷N. Beverini, G. Carelli, A. De Michele, A. Moretti, L. Mahler, A. Tredicucci, H. E. Beere, and D. A. Ritchie, "Frequency characterization of a terahertz quantum-cascade laser," *IEEE Trans. Instrum. Meas.* **56**, 262 (2007).

³⁸L. Schrottke, X. Lü, B. Röben, K. Biermann, M. Wienold, H. Richter, H.-W. Hübers, and H. T. Grahn, "Intrinsic frequency tuning of terahertz quantum-cascade lasers," *J. Appl. Phys.* **123**, 213102 (2018).

³⁹L. Gao, L. Zhao, J. L. Reno, and S. Kumar, "Electrical tuning of a terahertz quantum cascade laser based on detuned intersubband absorption," *Appl. Phys. Lett.* **115**, 141102 (2019).